Hindawi
Mathematical Problems in Engineering
Volume 2022, Article ID 1832525, 15 pages
https://doi.org/10.1155/2022/1832525

Research Article

Efficient Analytical Model for Time-Dependent Behavior of Layered Functionally Graded Plates with Viscoelastic Interlayers

Pengfei Liu,[1] **Peng Wu**,[2] **and Zhimin Wu**[1]

[1]*Institute of Civil and Architectural Engineering, Tongling University, Tongling 244000, China*
[2]*College of Civil Engineering, Nanjing Tech University, Nanjing 211816, China*

Correspondence should be addressed to Pengfei Liu; tlliupengfei@tlu.edu.cn

Received 5 March 2022; Accepted 4 May 2022; Published 28 May 2022

Academic Editor: Rossana Dimitri

Layered functionally graded (FG) plate plays an important role in engineering constructions. In this work, an efficient analytical solution is proposed to investigate the time-dependent characters of layered FG plate with viscoelastic interlayers, in which each FG layer is described by the elasticity theory, and the interlayer viscoelasticity is simulated by the generalized Maxwell model. The constitutive equations in the interlayer are simplified, and then, the analytical solutions of stresses and displacements for the layered FG plate are solved by virtue of the efficient recursive matrix method. Some examples are analyzed to investigate the influences of geometric and material characteristics on the long-term behaviors for the FG plate.

1. Introduction

The layered plates are commonly used in various engineering [1–4], by right of their outstanding merits, such as high strength, lightweight, and corrosion resistance. Enough bonding stiffness between adjacent members is the guarantee of mechanical performance of layered plates. In many cases, the connection between adjacent layers is not rigid, and thus, the interfacial slip often happens [5, 6]. Besides, the bond behavior in layered plates exhibits viscoelastic property, due to the use of polymer adhesive [7, 8]. As a result, the mechanical performance of the whole layered plates is time-dependent under sustained loads [9].

Although the layered plates exhibit good mechanical performance, it is necessary to reduce immediately the modulus difference between adjacent layers, which is a major cause of large interlaminar stress [10]. This requirement has led to the development of a novel material, called functionally graded (FG) materials, which can be designed to have continuous mechanical properties [11–13]. Due to its outstanding behaviors, FG materials have been applied in various areas, such as piezoelectric fiber-reinforced composite [14], heat-resistant materials [15], and nonuniform porous materials [16]. The concept of FG materials has also been introduced into the layered plates as face and/or transition layers, which can optimize the stress distribution and deformation [17, 18].

A number of works have been proposed to study the mechanical responses of layered FG plates. Gunes et al. [19] presented a backpropagation artificial neural network method for investigating the three-dimensional free vibration response of an adhesively bonded wide and narrow FG plates. Demirbas and Apalak [20] performed a thermoelastic investigation of FG circular plates with adhesive bond and gave the thermal stress and strain distributions with different gradient indexes. Based on the equivalent single-layer higher-order theory, Tornabene et al. [21] analyzed the dynamic response of anisotropic doubly curved shells with arbitrary geometry and variable thickness. According to the four-variable refined plate theory, an analytical solution was deduced by Li et al. [22] for the thermomechanical bending analysis of FG sandwich plate. Wang et al. [23] derived an analytical solution for investigating the heat transfer behavior in FG Sandwich plates. Tornabene et al. [24, 25] used the higher-order theory to study the dynamic behavior of anisotropic doubly curved shells. An extended cohesive damage model was proposed by Ghimire and Chen [26] for the analysis of geometrical ratio influences on the failure

mechanisms of FG sandwiches, and they found that the layered core can provide significant improvements in loading capacity. On the basis of the four-variable plate theory, Trinh el al. [27] presented a Levy solution with state space concept for static, dynamic, and buckling analyses for sandwich FG plates. Khorshidi and Karimi [28] established an analytical model based on a modified shear deformation theory for flutter investigation of sandwich plates with FG face sheets under thermal condition. A full layerwise method was employed by Nikbakht et al. [29] to obtain the yielding initiation of FG sandwich plates subjected to bi-sinusoidal distributed loading under general boundary conditions. Based on the first-order shear deformation theory, Tornabene [30] investigated the dynamic behavior of moderately thick functionally graded conical, cylindrical shells, and annular plates.

In the above literature, most works in regard to layered plates were based on the assumption of perfectly bonding or static slip, while the time-dependent characters resulting from viscoelastic bonding interlayers were neglected. Furthermore, the solutions based on the simplified plate theories have considerable error for thick plates.

This work proposes an efficient analytical model for investigating the time-dependent bending behavior of layered FG plates with considering viscoelastic bonding interlayer. In the analytical model, the mechanical behavior of each FG layer is expressed by the three-dimensional elasticity theory, which renounces the shear deformation assumption. Thus, it is highly accurate for structures with any thickness. The interlayer viscoelasticity is described by the generalized Maxwell model. The constitutive equations in the interlayer are simplified, and then, the analytical solutions of stresses and displacements for the layered FG plate are solved by virtue of the efficient recursive matrix method. Additionally, some examples provided by the present solution are conducted to investigate the influences of geometric and material characteristics on the time-dependent behaviors of the FG plate.

2. Efficient Analytical Model

In Figure 1, a layered FG plate formed by p FG layers bonded by viscoelastic bonding interlayer is considered, which is simply supported and bears to a sustained load $q(x,y)$ on its top. The three-dimensional size of the plate is $a \times b \times H$, and the thicknesses for FG layer and bonding interlayer are, respectively, h_i and Δh, in which the label i means the layer index. The elastic modulus of each FG layer, denoted by $E_i(z)$, varies according to the exponential law along the thickness direction, and is expressed by

$$E_i(z) = E_0^i e^{k_i\left(z-d_i^b\right)}, \tag{1}$$

where k_i is the graded index and $E_0^i = E_i(d_i^b)$. The generalized Maxwell model, as shown in Figure 2, is employed to model the interlayer viscoelasticity, with time-dependent shear modulus given by

$$G^*(t) = G_\infty + \sum_{j=1}^{n} G_j e^{(-t/\theta)_{G,j}}. \tag{2}$$

2.1. Governing Equations for a FG Layer. According to the elasticity theory, the constitutive equations for the ith ($i = 1, 2, \ldots, p$) FG layer are

$$\begin{aligned}
\sigma_x^i &= (\lambda_i + 2G_i)\varepsilon_x^i + \lambda_i\varepsilon_y^i + \lambda_i\varepsilon_z^i, \quad \tau_{yz}^i = G_i\gamma_{yz}^i,\\
\sigma_y^i &= \lambda_i\varepsilon_x^i + (\lambda_i + 2G_i)\varepsilon_y^i + \lambda_i\varepsilon_z^i, \quad \tau_{xz}^i = G_i\gamma_{xz}^i,\\
\sigma_z^i &= \lambda_i\varepsilon_x^i + \lambda_i\varepsilon_y^i + (\lambda_i + 2G_i)\varepsilon_z^i, \quad \tau_{xy}^i = G_i\gamma_{xy}^i,
\end{aligned} \tag{3}$$

where σ_x^i, σ_y^i, σ_z^i, τ_{xy}^i, τ_{yz}^i, and τ_{xz}^i are stresses, ε_x^i, ε_y^i, ε_z^i, γ_{xy}^i, γ_{yz}^i, and γ_{xz}^i are strains and λ_i and G_i are lame parameters expressed as follows:

$$\begin{aligned}
\lambda_i(z) &= \frac{\mu_i E_i(z)}{(1+\mu_i)(1-2\mu_i)},\\
G_i(z) &= \frac{E_i(z)}{2(1+\mu_i)}.
\end{aligned} \tag{4}$$

The strain-displacement relations are given by

$$\begin{aligned}
&\varepsilon_x^i = \frac{\partial u^i}{\partial x}, \varepsilon_y^i = \frac{\partial v^i}{\partial y}, \varepsilon_z^i = \frac{\partial w^i}{\partial z},\\
&\gamma_{xy}^i = \frac{\partial u^i}{\partial y} + \frac{\partial v^i}{\partial x}, \gamma_{yz}^i = \frac{\partial v^i}{\partial z} + \frac{\partial w^i}{\partial y}, \gamma_{xz}^i = \frac{\partial u^i}{\partial z} + \frac{\partial w^i}{\partial x},
\end{aligned} \tag{5}$$

where u^i, v^i, and w^i represent the displacements in x, y, and z direction, respectively. The stress components of each FG layer should meet the following static equilibrium equations:

$$\begin{aligned}
&\frac{\partial \sigma_x^i}{\partial x} + \frac{\partial \tau_{xy}^i}{\partial y} + \frac{\partial \tau_{xz}^i}{\partial z} = 0,\\
&\frac{\partial \sigma_y^i}{\partial y} + \frac{\partial \tau_{xy}^i}{\partial x} + \frac{\partial \tau_{yz}^i}{\partial z} = 0,\\
&\frac{\partial \sigma_z^i}{\partial z} + \frac{\partial \tau_{xz}^i}{\partial x} + \frac{\partial \tau_{yz}^i}{\partial y} = 0.
\end{aligned} \tag{6}$$

The simply supported boundary conditions can be expressed by

$$\begin{aligned}
v^i = w^i = \sigma_x^i &= 0, \quad at\, x = 0, a,\\
u^i = w^i = \sigma_x^i &= 0, \quad at\, y = 0, b.
\end{aligned} \tag{7}$$

Four steps are taken to obtain the differential equation involving displacement components. Firstly, by substituting (1) and (5) into (3) and eliminating the strain components, one has

$$\sigma_x^i = \frac{E_0^i e^{k_i(z-d_0^i)}}{(1+\mu_i)(1-2\mu_i)}\left[(1-\mu_i)\frac{\partial u^i}{\partial x} + \mu_i\frac{\partial v^i}{\partial y} + \mu_i\frac{\partial w^i}{\partial z}\right],$$

$$\sigma_y^i = \frac{E_0^i e^{k_i(z-d_0^i)}}{(1+\mu_i)(1-2\mu_i)}\left[\mu_i\frac{\partial u^i}{\partial x} + (1-\mu_i)\frac{\partial v^i}{\partial y} + \mu_i\frac{\partial w^i}{\partial z}\right],$$

$$\sigma_z^i = \frac{E_0^i e^{k_i(z-d_0^i)}}{(1+\mu_i)(1-2\mu_i)}\left[\mu_i\frac{\partial u^i}{\partial x} + \mu_i\frac{\partial v^i}{\partial y} + (1-\mu_i)\frac{\partial w^i}{\partial z}\right],$$

$$\tau_{xy}^i = \frac{E_0^i e^{k_i(z-d_0^i)}}{2(1+\mu_i)}\left(\frac{\partial u^i}{\partial y} + \frac{\partial v^i}{\partial x}\right), \tag{8}$$

$$\tau_{yz}^i = \frac{E_0^i e^{k_i(z-d_0^i)}}{2(1+\mu_i)}\left(\frac{\partial v^i}{\partial z} + \frac{\partial w^i}{\partial y}\right),$$

$$\tau_{xz}^i = \frac{E_0^i e^{k_i(z-d_0^i)}}{2(1+\mu_i)}\left(\frac{\partial u^i}{\partial z} + \frac{\partial w^i}{\partial x}\right).$$

By substituting (8) into (6) and eliminating the stress components, the governing equations only involving the displacement components are obtained:

$$\frac{2(1-\mu_i)}{(1-2\mu_i)}\frac{\partial^2 u^i}{\partial x^2} + \frac{\partial^2 u^i}{\partial y^2} + \frac{\partial^2 u^i}{\partial z^2} + k_i\frac{\partial u^i}{\partial z} + \frac{1}{(1-2\mu_i)}\frac{\partial^2 v^i}{\partial x\partial y} + \frac{1}{(1-2\mu_i)}\frac{\partial^2 w^i}{\partial x\partial z} + k_i\frac{\partial w^i}{\partial x} = 0,$$

$$\frac{1}{(1-2\mu_i)}\frac{\partial^2 u^i}{\partial x\partial y} + \frac{\partial^2 v^i}{\partial x^2} + \frac{2(1-\mu_i)}{(1-2\mu_i)}\frac{\partial^2 v^i}{\partial y^2} + \frac{\partial^2 v^i}{\partial z^2} + k_i\frac{\partial v^i}{\partial z} + \frac{1}{(1-2\mu_i)}\frac{\partial^2 w^i}{\partial y\partial z} + k_i\frac{\partial w^i}{\partial y} = 0, \tag{9}$$

$$\frac{1}{(1-2\mu_i)}\frac{\partial^2 u^i}{\partial x\partial z} + \frac{2k_i\mu_i}{(1-2\mu_i)}\frac{\partial u^i}{\partial x} + \frac{1}{(1-2\mu_i)}\frac{\partial^2 v^i}{\partial y\partial z} + \frac{2}{(1-2\mu_i)}k_i\mu_i\frac{\partial v^i}{\partial y} + \frac{\partial^2 w^i}{\partial x^2} + \frac{\partial^2 w^i}{\partial y^2} + \frac{2(1-\mu_i)}{(1-2\mu_i)}\frac{\partial^2 w^i}{\partial z^2} + \frac{2(1-\mu_i)}{(1-2\mu_i)}k_i\frac{\partial w^i}{\partial z} = 0.$$

The present structural problem is displacement-based, and the stresses can be determined by (8) after the displacements are solved. The above governing equations are actually partial differential equations which can hard to be solved directly. Secondly, for simply supported boundary conditions, the displacements of each FG layer can be expanded in Fourier series as follows:

$$\begin{bmatrix} u^i(x,y,z,t) \\ v^i(x,y,z,t) \\ w^i(x,y,z,t) \end{bmatrix} = \sum_{m=1}^{\infty}\sum_{n=1}^{\infty}\begin{bmatrix} u^{i,mn}(z,t)\cos(\alpha_m x)\sin(\beta_n y) \\ v^{i,mn}(z,t)\sin(\alpha_m x)\cos(\beta_n y) \\ w^{i,mn}(z,t)\sin(\alpha_m x)\sin(\beta_n y) \end{bmatrix}, \tag{10}$$

where $\alpha_m = m\pi/a$ and $\beta_n = n\pi/b$. Thirdly, by applying the Fourier series expansion of (10) to (9), the partial differential equations become ordinary differential equations as follows:

$$\frac{\partial^2 u^{i,mn}(z,t)}{\partial z^2} + k_i\frac{\partial u^{i,mn}(z,t)}{\partial z} - \left[\frac{2(1-\mu_i)}{(1-2\mu_i)}\alpha_m^2 + \beta_n^2\right]u^{i,mn}(z,t) - \frac{\alpha_m\beta_n}{(1-2\mu_i)}v^{i,mn}(z,t) + \frac{\alpha_m}{(1-2\mu_i)}\frac{\partial w^{i,mn}(z,t)}{\partial z}$$
$$+ k_i\alpha_m w^{i,mn}(z,t) = 0,$$

$$\begin{aligned}
&\frac{-\alpha_m\beta_n}{(1-2\mu_i)}u^{i,mn}(z,t)+\frac{\partial^2 v^{i,mn}(z,t)}{\partial z^2}+k_i\frac{\partial v^{i,mn}(z,t)}{\partial z}-\left[\alpha_m^2+\frac{2(1-\mu_i)}{(1-2\mu_i)}\beta_n^2\right]v^{i,mn}(z,t)+\frac{\beta_n}{(1-2\mu_i)}\frac{\partial w^{i,mn}(z,t)}{\partial z}\\
&\quad+k_i\beta_n w^{i,mn}(z,t)=0,\\
&\frac{\alpha_m}{2(1-\mu_i)}\frac{\partial u^{i,mn}(z,t)}{\partial z}+\frac{k_i\mu_i\alpha_m}{(1-\mu_i)}u^{i,mn}(z,t)+\frac{\beta_n}{2(1-\mu_i)}\frac{\partial v^{i,mn}(z,t)}{\partial z}+\frac{k_i\mu_i\beta_n}{(1-\mu_i)}v^{i,mn}(z,t)\\
&\quad-\frac{\partial^2 w^{i,mn}(z,t)}{\partial z^2}-k_i\frac{\partial w^{i,mn}(z,t)}{\partial z}+\frac{(1-2\mu_i)\left(\alpha_m^2+\beta_n^2\right)}{2(1-\mu_i)}w^{i,mn}(z,t)=0.
\end{aligned}\tag{11}$$

At last, a fourth-order differential equation of $w^{i,mn}$ is derived out by eliminating $u^{i,mn}$ and $v^{i,mn}$ in (11):

$$\begin{aligned}
&\frac{\partial^4 w^{i,mn}}{\partial z^4}+2k_i\frac{\partial^3 w^{i,mn}}{\partial z^3}+\left(k_i^2-2\alpha_{mn}^2\right)\frac{\partial^2 w^{i,mn}}{\partial z^2}\\
&\quad-2k_i\alpha_{mn}^2\frac{\partial w^{i,mn}}{\partial z}+\left(\alpha_{mn}^4+k^2\alpha_{mn}^2\frac{\mu_i}{1-\mu_i}\right)w^{i,mn}=0.
\end{aligned}\tag{12}$$

The general solution of $w^{i,mn}$ is

$$w_{mn}^i(z,t)=\sum_{j=1}^{4}e^{g_{mn}^{ij}z}C_{mn}^{ij}(t),\tag{13}$$

where $C_{mn,j}^i(t)$ are the undetermined time-dependent coefficients, which can be obtained according to the boundary and continuity conditions in the subsequent sections; the details of $g_{mn,j}^i$ are defined in Appendix A. By substituting into (13) and (11), $u^{i,mn}$ and $v^{i,mn}$ are obtained:

$$\begin{aligned}
u_{mn}^i(z,t)&=\sum_{j=1}^{4}f_{mn}^{ij}e^{g_{mn}^{ij}z}C_{mn}^{ij}(t)+\sum_{j=5}^{6}e^{g_{mn}^{ij}z}C_{mn}^{ij}(t),\\
v_{mn}^i(z,t)&=\frac{\beta_n}{\alpha_m}\sum_{j=1}^{4}f_{mn}^{ij}e^{g_{mn}^{ij}z}C_{mn}^{ij}(t)-\frac{\alpha_m}{\beta_n}\sum_{j=5}^{6}e^{g_{mn}^{ij}z}C_{mn}^{ij}(t),
\end{aligned}\tag{14}$$

where the details of f_{mn}^{ij} are listed in Appendix A. By substituting of (13), (14), and (8) into (9), the stress components involving undetermined coefficients can be written as

$$\begin{aligned}
\sigma_{x,mn}^i(z,t)&=\frac{E_0^ie^{k_i(z-d_0^i)}}{(1+\mu_i)(1-2\mu_i)}\left\{\sum_{j=1}^{4}\left[-\alpha_m(1-\mu_i)f_{mn}^{ij}-\frac{\mu_i\beta_n^2f_{mn}^{ij}}{\alpha_m}+\mu_ig_{mn}^{ij}\right]e^{g_{mn}^{ij}z}C_{mn}^{ij}(t)+\sum_{j=5}^{6}\alpha_m(2\mu_i-1)e^{g_{mn}^{ij}z}C_{mn}^{ij}(t)\right\},\\
\sigma_{y,mn}^i(z,t)&=\frac{E_0^ie^{k_i(z-d_0^i)}}{(1+\mu_i)(1-2\mu_i)}\left\{\sum_{j=1}^{4}\left[-\alpha_m\mu_if_{mn}^{ij}-\frac{(1-\mu_i)\beta_n^2f_{mn}^{ij}}{\alpha_m}+\mu_ig_{mn}^{ij}\right]e^{g_{mn}^{ij}z_i}C_{mn}^{ij}(t)+\sum_{j=5}^{6}\alpha_m(1-2\mu_i)e^{g_{mn}^{ij}z_i}C_{mn}^{ij}(t)\right\},\\
\sigma_{z,mn}^i(z,t)&=\frac{E_0^ie^{k_i(z-d_0^i)}}{(1+\mu_i)(1-2\mu_i)}\sum_{j=1}^{4}\left[-\alpha_m\mu_if_{mn}^{ij}-\frac{\mu_i\beta_n^2f_{mn}^{ij}}{\alpha_m}+(1-\mu_i)g_{mn}^{ij}\right]e^{g_{mn}^{ij}z}C_{mn}^{ij}(t),\\
\tau_{xy,mn}^i(z,t)&=\frac{E_0^ie^{k_i(z-d_0^i)}}{2(1+\mu_i)}\left[\sum_{j=1}^{4}2\beta_nf_{mn}^{ij}e^{g_{mn}^{ij}z}C_{mn}^{ij}(t)+\sum_{j=5}^{6}\left(\beta_n-\frac{\alpha_m^2}{\beta_n}\right)e^{g_{mn}^{ij}z}C_{mn}^{ij}(t)\right],\\
\tau_{yz,mn}^i(z,t)&=\frac{E_0^ie^{k_i(z-d_0^i)}}{2(1+\mu_i)}\left[\sum_{j=1}^{4}\left(\frac{\beta_nf_{mn}^{ij}g_{mn}^{ij}}{\alpha_m}+\beta_n\right)e^{g_{mn}^{ij}z}C_{mn}^{ij}(t)-\sum_{j=5}^{6}\frac{\alpha_mg_{mn}^{ij}}{\beta_n}e^{g_{mn}^{ij}z}C_{mn}^{ij}(t)\right],\\
\tau_{xz,mn}^i(z,t)&=\frac{E_0^ie^{k_i(z-d_0^i)}}{2(1+\mu_i)}\left[\sum_{j=1}^{4}\left(f_{mn}^{ij}g_{mn}^{ij}+\alpha_m\right)e^{g_{mn}^{ij}z}C_{mn}^{ij}(t)+\sum_{j=5}^{6}g_{mn}^{ij}e^{g_{mn}^{ij}z}C_{mn}^{ij}(t)\right].
\end{aligned}\tag{15}$$

2.2. Governing Equations for a Viscoelastic Interlayer. According to the Boltzmann superposition principle, the constitutive equations for the ith ($i = 1, 2, \ldots, p$-1) interlayer are given by

$$\tau_{xz}^{*i}(x,y,t) = \int_{-\infty}^{t} G^{*}(t-\xi)\frac{\partial \gamma_{xz}^{i*}(x,y,\xi)}{\partial \xi}\mathrm{d}\xi,$$
$$\tau_{yz}^{*i}(x,y,t) = \int_{-\infty}^{t} G^{*}(t-\xi)\frac{\partial \gamma_{yz}^{i*}(x,y,\xi)}{\partial \xi}\mathrm{d}\xi. \tag{16}$$

The above convolution integral equations means that the stress of viscoelastic interlayer depends on the total strain history, which leads to the heavy calculation and time-consuming. In the present work, they are simplified as

$$\tau_{xz}^{i*}(x,y,t) = G^{*}(t)\gamma_{xz}^{i*}(x,y,t),$$
$$\tau_{yz}^{i*}(x,y,t) = G^{*}(t)\gamma_{yz}^{i*}(x,y,t). \tag{17}$$

In comparison with the exact solution, this simplification leads to small error, and the present solution is always on the side of safety [25]. Considering that Δh is far less than h_i, the shear strains can be assumed to be constant in z direction and given by

$$\gamma_{xz}^{i*}(x,y,t) = \frac{u^{i+1}\left(x,y,d_{i+1}^{b},t\right) - u^{i}\left(x,y,d_{i}^{t},t\right)}{\Delta h},$$
$$\gamma_{yz}^{i*}(x,y,t) = \frac{v^{i+1}\left(x,y,d_{i+1}^{b},t\right) - v^{i}\left(x,y,d_{i}^{t},t\right)}{\Delta h}. \tag{18}$$

The shear stress continuity relationships between adjacent layers are

$$\tau_{xz}^{i}\left(x,y,d_{i}^{t},t\right) = \tau_{xz}^{i*}(x,y,t) = \tau_{xz}^{i+1}\left(x,y,d_{i+1}^{b},t\right),$$
$$\tau_{yz}^{i}\left(x,y,d_{i}^{t},t\right) = \tau_{yz}^{i*}(x,y,t) = \tau_{yz}^{i+1}\left(x,y,d_{i+1}^{b},t\right). \tag{19}$$

2.3. Recursive Matrix Method. The stresses on the top and bottom surfaces of the plate are

$$\begin{aligned}
\sigma_{z}^{p}(x,y,H,t) &= -q(x,y),\\
\tau_{xz}^{p}(x,y,H,t) &= 0,\\
\tau_{yz}^{p}(x,y,H,t) &= 0,\\
\sigma_{z}^{1}(x,y,0,t) &= 0,\\
\tau_{xz}^{1}(x,y,0,t) &= 0,\\
\tau_{yz}^{1}(x,y,0,t) &= 0.
\end{aligned} \tag{20}$$

Since the stresses and displacements are in series form, $q(x,y)$ should also be expanded as

$$q(x,y) = \sum_{m=1}^{\infty}\sum_{n=1}^{\infty} q_{mn}\sin(\alpha_m x)\sin(\beta_n y),$$
$$q_{mn} = -\frac{4}{ab}\int_{0}^{a}\int_{0}^{b} q(x,y)\sin(\alpha_m x)\sin(\beta_n y)\mathrm{d}x\mathrm{d}y. \tag{21}$$

By substitution of (13)–(15) into (8), the general solution of stresses and displacements can be transferred into the matrix form as

$$\mathbf{\Phi}_{mn}^{i}(z,t) = \mathbf{M}_{mn}^{i}(z)\mathbf{\Lambda}_{mn}^{i}(t), \tag{22}$$

where

$$\begin{aligned}
\mathbf{\Phi}_{mn}^{i}(z,t) &= \left[\, u^{i,mn}(z,t)\ \ v^{i,mn}(z,t)\ \ w^{i,mn}(z,t)\ \ \sigma_{z}^{i,mn}(z,t)\ \ \tau_{xz}^{i,mn}(z,t)\ \ \tau_{yz}^{i,mn}(z,t)\,\right]^{T},\\
\mathbf{\Lambda}_{mn}^{i}(t) &= \left[\, C_{mn,1}^{i}(t)\ \ C_{mn,2}^{i}(t)\ \ C_{mn,3}^{i}(t)\ \ C_{mn,4}^{i}(t)\ \ C_{mn,5}^{i}(t)\ \ C_{mn,6}^{i}(t)\,\right]^{T},\\
\mathbf{M}_{mn}^{i}(z) &= \begin{bmatrix}
R_{\mathrm{mn}}^{11}(z) & R_{\mathrm{mn}}^{12}(z) & R_{\mathrm{mn}}^{13}(z) & R_{\mathrm{mn}}^{14}(z) & R_{\mathrm{mn}}^{15}(z) & R_{\mathrm{mn}}^{16}(z)\\
R_{\mathrm{mn}}^{21}(z) & R_{\mathrm{mn}}^{22}(z) & R_{\mathrm{mn}}^{23}(z) & R_{\mathrm{mn}}^{24}(z) & R_{\mathrm{mn}}^{25}(z) & R_{\mathrm{mn}}^{26}(z)\\
R_{\mathrm{mn}}^{31}(z) & R_{\mathrm{mn}}^{32}(z) & R_{\mathrm{mn}}^{33}(z) & R_{\mathrm{mn}}^{34}(z) & 0 & 0\\
R_{\mathrm{mn}}^{41}(z) & R_{\mathrm{mn}}^{42}(z) & R_{\mathrm{mn}}^{43}(z) & R_{\mathrm{mn}}^{44}(z) & 0 & 0\\
R_{\mathrm{mn}}^{51}(z) & R_{\mathrm{mn}}^{52}(z) & R_{\mathrm{mn}}^{53}(z) & R_{\mathrm{mn}}^{54}(z) & R_{\mathrm{mn}}^{55}(z) & R_{\mathrm{mn}}^{56}(z)\\
R_{\mathrm{mn}}^{61}(z) & R_{\mathrm{mn}}^{62}(z) & R_{\mathrm{mn}}^{63}(z) & R_{\mathrm{mn}}^{64}(z) & R_{\mathrm{mn}}^{65}(z) & R_{\mathrm{mn}}^{66}(z)
\end{bmatrix},
\end{aligned} \tag{23}$$

where the nonzero coefficients in matrix $\mathbf{M}_{mn}^{i}(z)$ can be found in Appendix B. By combining (17)–(19), the continuity relationships between the adjacent FG layers are rewritten in the matrix form as

$$\mathbf{\Phi}_{mn}^{i+1}\left(d_{i+1}^{b},t\right) = \mathbf{\Psi}(t)\mathbf{\Phi}_{mn}^{i}\left(d_{i}^{t},t\right), \tag{24}$$

where

$$\mathbf{\Psi}(t)=\begin{bmatrix} 1 & 0 & -\Delta h\alpha_{\mathrm{m}} & 0 & \dfrac{\Delta h}{G^{*}(t)} & 0 \\ 0 & 1 & -\Delta h\beta_{\mathrm{n}} & 0 & 0 & \dfrac{\Delta h}{G^{*}(t)} \\ 0 & 0 & 1 & 0 & 0 & 0 \\ 0 & 0 & 0 & 1 & 0 & 0 \\ 0 & 0 & 0 & 0 & 1 & 0 \\ 0 & 0 & 0 & 0 & 0 & 1 \end{bmatrix}. \tag{25}$$

By substituting d_i^b and d_i^t into the z-coordinate in (24), respectively, we obtain

$$\begin{aligned} \mathbf{\Phi}_{mn}^{i}\left(d_i^b,t\right) &= \mathbf{M}_{mn}^{i}\left(d_i^b\right)\mathbf{\Lambda}_{mn}^{i}(t), \\ \mathbf{\Phi}_{mn}^{i}\left(d_i^t,t\right) &= \mathbf{M}_{mn}^{i}\left(d_i^t\right)\mathbf{\Lambda}_{mn}^{i}(t). \end{aligned} \tag{26}$$

Elimination of $\Lambda_{mn}^{i}(t)$ in (26) yields

$$\mathbf{\Phi}_{mn}^{i}\left(d_i^t,t\right)=\left[\mathbf{M}_{mn}^{i}\left(d_i^t\right)\mathbf{M}_{mn}^{i}\left(d_i^b\right)^{-1}\right]\mathbf{\Phi}_{mn}^{i}\left(d_i^b,t\right). \tag{27}$$

By reusing (24) and (27), from $i=1$ to $i=p$, one obtains

$$\begin{aligned} \mathbf{\Phi}_{mn}^{p}\left(d_p^t,t\right) = &\prod_{i=p}^{2}\left[\mathbf{M}_{mn}^{i}\left(d_i^t\right)\mathbf{M}_{mn}^{i}\left(d_i^b\right)^{-1}\mathbf{\Psi}(t)\right]\mathbf{M}_{mn}^{1}\left(d_1^t\right)\mathbf{M}_{mn}^{1} \\ &\cdot\left(d_1^b\right)^{-1}\mathbf{\Phi}_{mn}^{1}\left(d_1^b,t\right). \end{aligned} \tag{28}$$

Four 3×3, submatrices are used to define the matrix multiplication in (28) as follows:

$$\begin{aligned} \begin{bmatrix} \mathbf{C}_{mn,11}^{i} & \mathbf{C}_{mn,12}^{i} \\ \mathbf{C}_{mn,21}^{i} & \mathbf{C}_{mn,22}^{i} \end{bmatrix} = &\prod_{i=p}^{2}\left[\mathbf{M}_{mn}^{i}\left(d_i^t\right)\mathbf{M}_{mn}^{i}\left(d_i^b\right)^{-1}\mathbf{\Psi}(t)\right]\mathbf{M}_{mn}^{1} \\ &\cdot\left(d_1^t\right)\mathbf{M}_{mn}^{1}\left(d_1^b\right)^{-1}. \end{aligned} \tag{29}$$

Thus, (28) can be written as

$$\mathbf{\Phi}_{mn}^{p}\left(d_p^t,t\right)=\begin{bmatrix} \mathbf{C}_{mn,11}^{i} & \mathbf{C}_{mn,12}^{i} \\ \mathbf{C}_{mn,21}^{i} & \mathbf{C}_{mn,22}^{i} \end{bmatrix}\mathbf{\Phi}_{mn}^{p}\left(d_p^t,t\right). \tag{30}$$

By the decomposition of (30), two submatrix equations are given as

$$\begin{aligned} \begin{bmatrix} u^{p,mn}\left(d_1^b,t\right) \\ v_{xz}^{p,mn}\left(d_1^b,t\right) \\ w_{yz}^{p,mn}\left(d_1^b,t\right) \end{bmatrix} &= \mathbf{C}_{mn,11}^{i}\begin{bmatrix} u^{1,mn}\left(d_1^b,t\right) \\ v_{xz}^{1,mn}\left(d_1^b,t\right) \\ w_{yz}^{1,mn}\left(d_1^b,t\right) \end{bmatrix} + \mathbf{C}_{mn,12}^{i}\begin{bmatrix} \sigma_z^{1,mn}\left(d_1^b,t\right) \\ \tau_{xz}^{1,mn}\left(d_1^b,t\right) \\ \tau_{yz}^{1,mn}\left(d_1^b,t\right) \end{bmatrix}, \\ \begin{bmatrix} \sigma_z^{p,mn}\left(d_1^b,t\right) \\ \tau_{xz}^{p,mn}\left(d_1^b,t\right) \\ \tau_{yz}^{p,mn}\left(d_1^b,t\right) \end{bmatrix} &= \mathbf{C}_{mn,21}^{i}\begin{bmatrix} u^{1,mn}\left(d_1^b,t\right) \\ v_{xz}^{1,mn}\left(d_1^b,t\right) \\ w_{yz}^{1,mn}\left(d_1^b,t\right) \end{bmatrix} + \mathbf{C}_{mn,22}^{i}\begin{bmatrix} \sigma_z^{1,mn}\left(d_1^b,t\right) \\ \tau_{xz}^{1,mn}\left(d_1^b,t\right) \\ \tau_{yz}^{1,mn}\left(d_1^b,t\right) \end{bmatrix}. \end{aligned} \tag{31}$$

By solving (31), the displacement boundary value on the bottom surface of the structure can be expressed as

$$\begin{bmatrix} u^{1,mn}\left(d_1^b,t\right) \\ v_{xz}^{1,mn}\left(d_1^b,t\right) \\ w_{yz}^{1,mn}\left(d_1^b,t\right) \end{bmatrix} = \left(\mathbf{C}_{mn,21}^{i}\right)^{-1}\begin{bmatrix} q_{mn} \\ 0 \\ 0 \end{bmatrix}. \tag{32}$$

Similar to the relationship in (28), $\Phi_{mn}^{i}(d_i^t,t)$ for any FG layer is obtained from (24) and (27) as follows:

$$\begin{aligned} \mathbf{\Phi}_{mn}^{i}\left(d_i^t,t\right) = &\prod_{j=i}^{2}\left[\mathbf{M}_{mn}^{j}\left(d_j^t\right)\mathbf{M}_{mn}^{j}\left(d_j^t\right)^{-1}\Psi(t)\right]\mathbf{M}_{mn}^{1}\left(d_j^t\right)\mathbf{M}_{mn}^{1} \\ &\cdot\left(d_j^t\right)^{-1}\mathbf{\Phi}_{mn}^{1}\left(d_1^b,t\right). \end{aligned} \tag{33}$$

The time-dependent coefficients of the ith FG layer are further obtained as

$$\begin{aligned} \mathbf{\Lambda}_{mn}^{i}(t) = &\mathbf{M}_{mn}^{i}\left(d_1^t\right)^{-1}\left[\prod_{j=i}^{2}\mathbf{M}_{mn}^{j}\left(d_1^t\right)\mathbf{M}_{mn}^{j}\left(d_1^t\right)^{-1}\mathbf{\Psi}(t)\right] \\ &\cdot\left[\mathbf{M}_{mn}^{1}\left(d_1^t\right)\mathbf{M}_{mn}^{1}\left(d_1^t\right)^{-1}\right]\mathbf{\Phi}_{mn}^{1}\left(d_1^b,t\right). \end{aligned} \tag{34}$$

Finally, the substitution of (34) into (13)–(15) yields the solution of stress and displacement components for each FG layer.

3. Numerical Results and Discussion

In the following, the FG sandwich plate ($p=3$) is taken as an example. The variables with the superscript r, e.g., σ_x^r, are defined as the result of stress or displacement at the point of $x=0\cdot 25a$, $y=0\cdot 25b$, and $z=h_1$. The variables with two vertical lines denote their absolute values, e.g., $|wi|$.

3.1. Validation of the Present Solution. The convergence property of the present solution is assessed first. The series are truncated into a finite number M for actual calculations

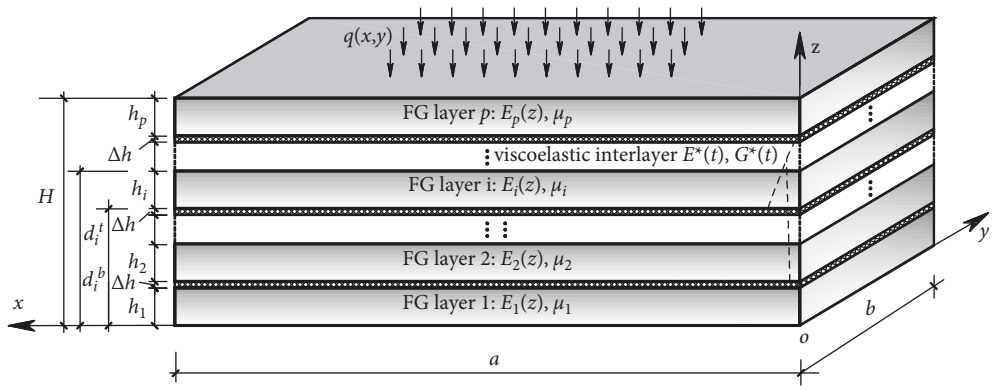

Figure 1: Schematic diagram of the layered FG plate bonded by the viscoelastic interlayer.

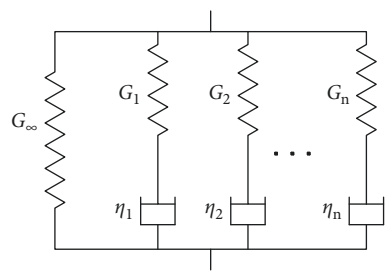

Figure 2: The configuration of the generalized Maxwell model ($\theta_i = \eta_i/G_j$).

here. The parameters in the FG plate are taken as $q(x,y) = 1\,\mathrm{N/mm^2}$, $a = 1000\,\mathrm{mm}$, $b = 800\,\mathrm{mm}$, $\Delta h = 0.5\,\mathrm{mm}$, $h_1 = h_3 = 30\,\mathrm{mm}$, $h_2 = 40\,\mathrm{mm}$, $E_0^1 = E_0^3 = 80\,\mathrm{GPa}$, $E_0^2 = 40\,\mathrm{GPa}$, $k_1 = k_3 = 0.05$, $k_2 = 0$, and $\mu_1 = \mu_2 = \mu_3 = \mu^* = 0.3$. The material of polyvinyl butyral (PVB) is chosen for the viscoelastic interlayer and its viscoelastic parameters of which are given in Table 1. Table 2 lists the present results with different series terms, respectively. It is found that the present results tend to be constant as series terms increase, and the convergence accuracy is four significant digits.

The present solution is compared with the Kirchhoff–Love (KL) solution [26], respectively. The parameters in the FG plate are fixed at $q(x,y) = \sin(\pi x/a)\sin(\pi y/b)\ \mathrm{N/mm^2}$, $a = b = 1000\,\mathrm{mm}$, $\Delta h = 0.2\,\mathrm{mm}$, $k_2 = 0$, $E_0^3 = E_0^1 e^{k_1 h_1} = 80\,\mathrm{GPa}$, $E_0^2 = 40\,\mathrm{GPa}$, $\mu_1 = \mu_2 = \mu_3 = \mu^* = 0.3$, $t = 10^4\,\mathrm{s}$, $G_\infty^* = 0.5\,\mathrm{MPa}$, $G_1^* = 500\,\mathrm{MPa}$, $\theta_{G,1} = 1\,\mathrm{s}$, $h_1{:}h_2{:}h_3 = 1:2{:}1$, and $k_3 = -k_1$. The above parameters mean that the geometric and material properties of the present structure are symmetric about the midplane in the direction of thickness. Figure 3 represents the relative error between KL solution and the present one for a different length-to-height ratio a/H and graded index k_1, respectively. A good agreement is found for KL solution in thin plate case with small $|k_1|$, while the relative error of KL results increases gradually as the plate become thick or k_1 decreases. The errors for σ_x^r, τ_{xz}^r, and w^r are 15.4%, 6.6%, and 15.9%, respectively, as $a/H = 8$ and $k_1 = -0.09$. The imprecision of KL solutions mainly results from the neglect of the transverse shear deformation and the deviation of neutral plane of the FG layer.

3.2. Parameter Research. In this section, some examples provided by the present solution are conducted to investigate the influences of geometric and material characteristics on the time-dependent behaviors of the FG plate. Some of the parameters are fixed at $q(x,y) = \sin(\pi x/a)\sin(\pi y/b)\ \mathrm{N/mm^2}$, $a = b = 1000\,\mathrm{mm}$, $k_1{:}k_3 = -1$, $k_2 = 0$, $E_0^3 = E_0^1 e^{k_1 h_1}$, $E_0^2 = 25\mathrm{Gpa}$, and $\mu_1 = \mu_2 = \mu_3 = \mu^* = 0.3$; the viscoelastic constants are given in Table 1, while the others are variable.

Figure 4 plots the stress and displacement distribution in z direction when $t = 1$ day, 1 year, and 10 years and the corresponding results in perfectly bonded (PB) case. The constants are fixed at $h_1 = h_3 = 20\,\mathrm{mm}$, $h_2 = 40\,\mathrm{mm}$, $\Delta h = 0.2\,\mathrm{mm}$, and $k_1 = -0.05$. It can be obtained from Figure 4 that $|\sigma_x^i|$, $|\tau_{xz}^i|$, $|\tau_{xy}^i|$, $|u^i|$, and $|w^i|$ considerably increase with t, while $|\sigma_y^i|$ changes slightly with time. σ_x^i and τ_{xy}^i show zig-zag distributions, and they, in the facial layers, are obviously curve distribution, which is different from isotropic material. u^i also show a zig-zag distribution but keeps straight in each FG layer. τ_{xz}^i gives a multipeak distribution. Compared with the results of PB case, the maximum values of $|\sigma_x^i|$, $|\tau_{xz}^i|$, $|\tau_{xy}^i|$, $|u^i|$, and $|w^i|$ increase by 200.1%, 26.2%, 200.2%, 604.7%, and 1221%, respectively, at $t = 10$ years.

The effect of the graded index on the stress and displacement of the FG plate, as well as the elastic modulus distributions along the thickness direction, are illustrated in Figure 5. The parameters are taken as $h_1 = h_3 = 10\,\mathrm{mm}$, $h_2 = 30\,\mathrm{mm}$, $\Delta h = 0.2\,\mathrm{mm}$, and $t = 1$ day, and the average modulus of FG facial layer, i.e., $(\int_0^{h_i} E_0^i e^{k_i y}\mathrm{d}y)/h_i$ $(i = 1,\ 3)$, is fixed at 80 GPa. From the

Table 1: The relaxation moduli and relaxation time of the generalized Maxwell model for PVB material.

J	G_j^* (MPa)	$\theta_{G,j}$ (s)
1	75.6426	3.256×10^{-11}
2	37.0677	4.949×10^{-9}
3	137.1552	7.243×10^{-8}
4	33.5140	9.864×10^{-6}
5	126.6048	2.806×10^{-3}
6	42.1950	1.644×10^{-1}
7	14.2162	2.265×10^{0}
8	3.5822	3.536×10^{1}
9	0.4538	9.368×10^{3}
10	0.1912	6.414×10^{5}
11	0.2893	4.135×10^{7}
∞	0.0880	

Table 2: Convergence analysis of the present method as $t=1$ day, 1 year, and 10 years, respectively.

T	M	u^r (mm)	w^r (mm)	σ_x^r (MPa)	σ_z^r (MPa)	τ_{xy}^r (MPa)	τ_{xz}^r (MPa)
1 day	1	0.03731	−1.068	−67.96	−0.2896	40.41	−0.1065
	5	0.03582	−1.088	−74.98	−0.3933	38.20	−0.1009
	9	0.03583	−1.088	−74.94	−0.3916	38.20	−0.1010
	13	0.03583	−1.088	−74.94	−0.3916	38.20	−0.1010
1 year	1	0.04072	−1.152	−74.16	−0.3056	44.10	−0.04183
	5	0.03866	−1.180	−83.43	−0.4379	41.03	−0.03940
	9	0.03867	−1.180	−83.30	−0.4307	41.04	−0.03946
	13	0.03867	−1.180	−83.30	−0.4310	41.04	−0.03946
10 years	1	0.04226	−1.190	−76.97	−0.3129	45.77	−0.01196
	5	0.03977	−1.222	−87.06	−0.4366	42.20	−0.01121
	9	0.03984	−1.222	−86.65	−0.4143	42.23	−0.01124
	13	0.03983	−1.222	−86.67	−0.4164	42.23	−0.01124

Note. M means the series terms.

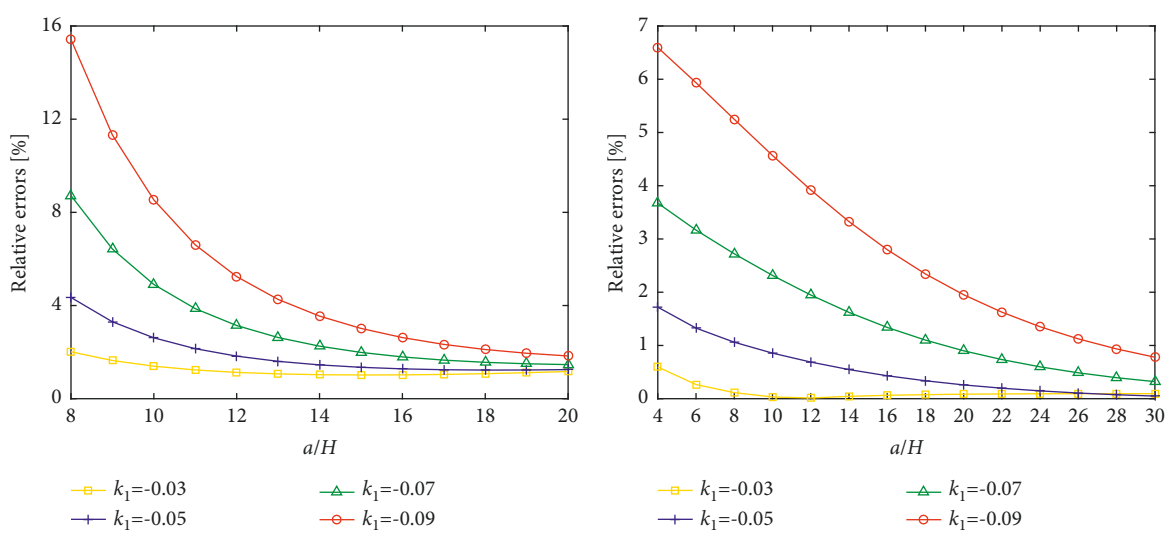

Figure 3: Continued.

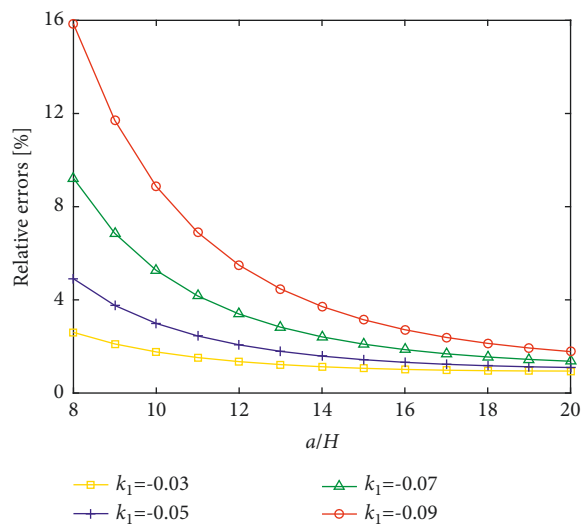

(c)

Figure 3: Relative errors of the KL solution compared with the present one for different length-to-height ratios as $k_1 = -0.03$, -0.05, -0.07, and -0.09 when $t = 10000$ s. *Note*. The errors are defined by $|[(\text{KL})\text{-Present}]/\text{Present}| \times 100\%$. (a) σ_x^r, (b) τ_{xz}^r, and (c) w^r.

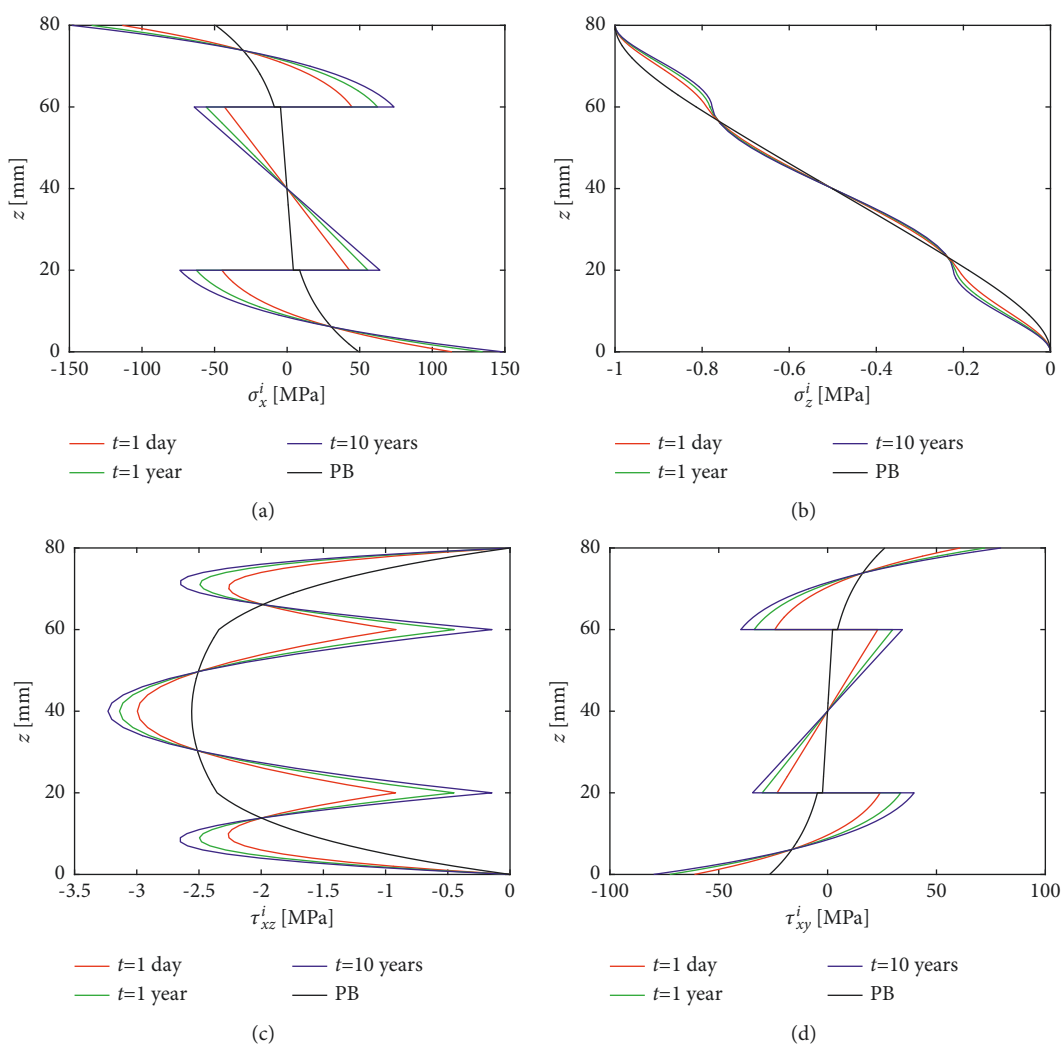

Figure 4: Continued.

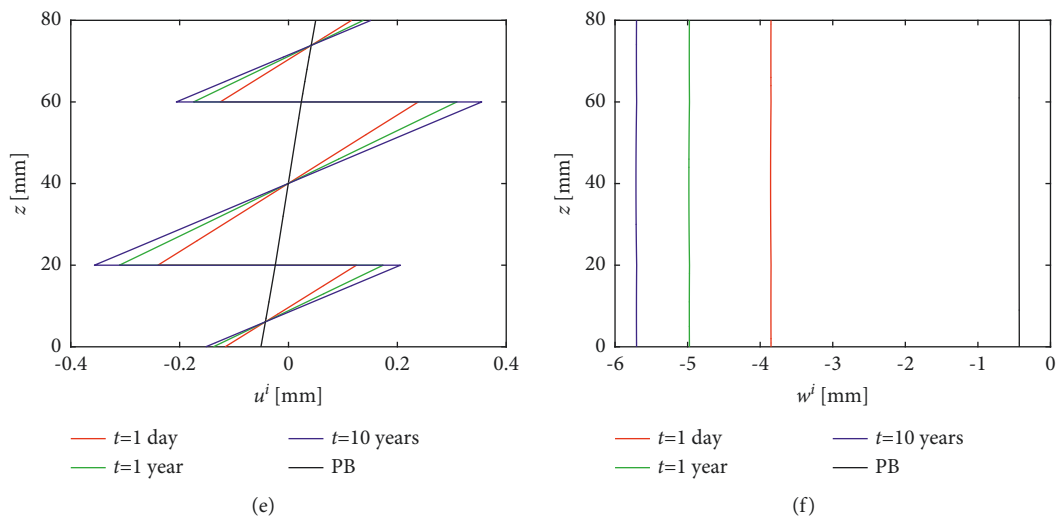

Figure 4: The distribution of the stress and displacement in the thickness direction at different time periods. (a) σ_x^i $(x = 0.5a, y = 0.5b)$, (b) σ_y^i $(x = 0.5a, y = 0.5b)$, (c) τ_{xz}^i $(x = 0, y = 0.5b)$, (d) τ_{xz}^i $(x = 0, y = 0)$, (e) u^i $(x = 0, y = 0.5b)$, and (f) w^i $(x = 0.5a, y = 0.5b)$.

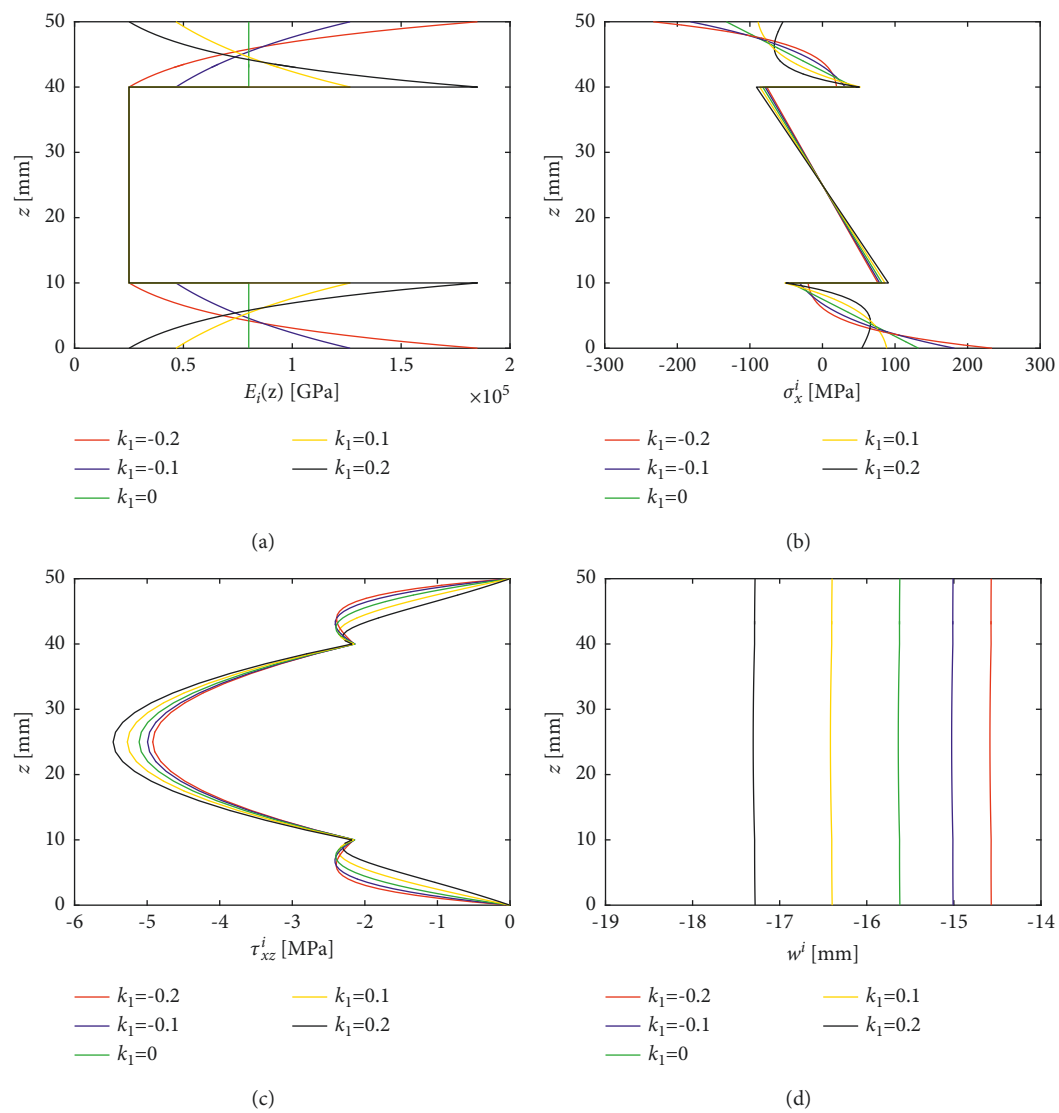

Figure 5: The influence of graded index on the distribution of the elastic modulus, stress, and displacement along the thickness direction with fixed material consumption. (a) $E_i(z)$, (b) σ_x^i, (c) τ_{xz}^i, and (d) w^i.

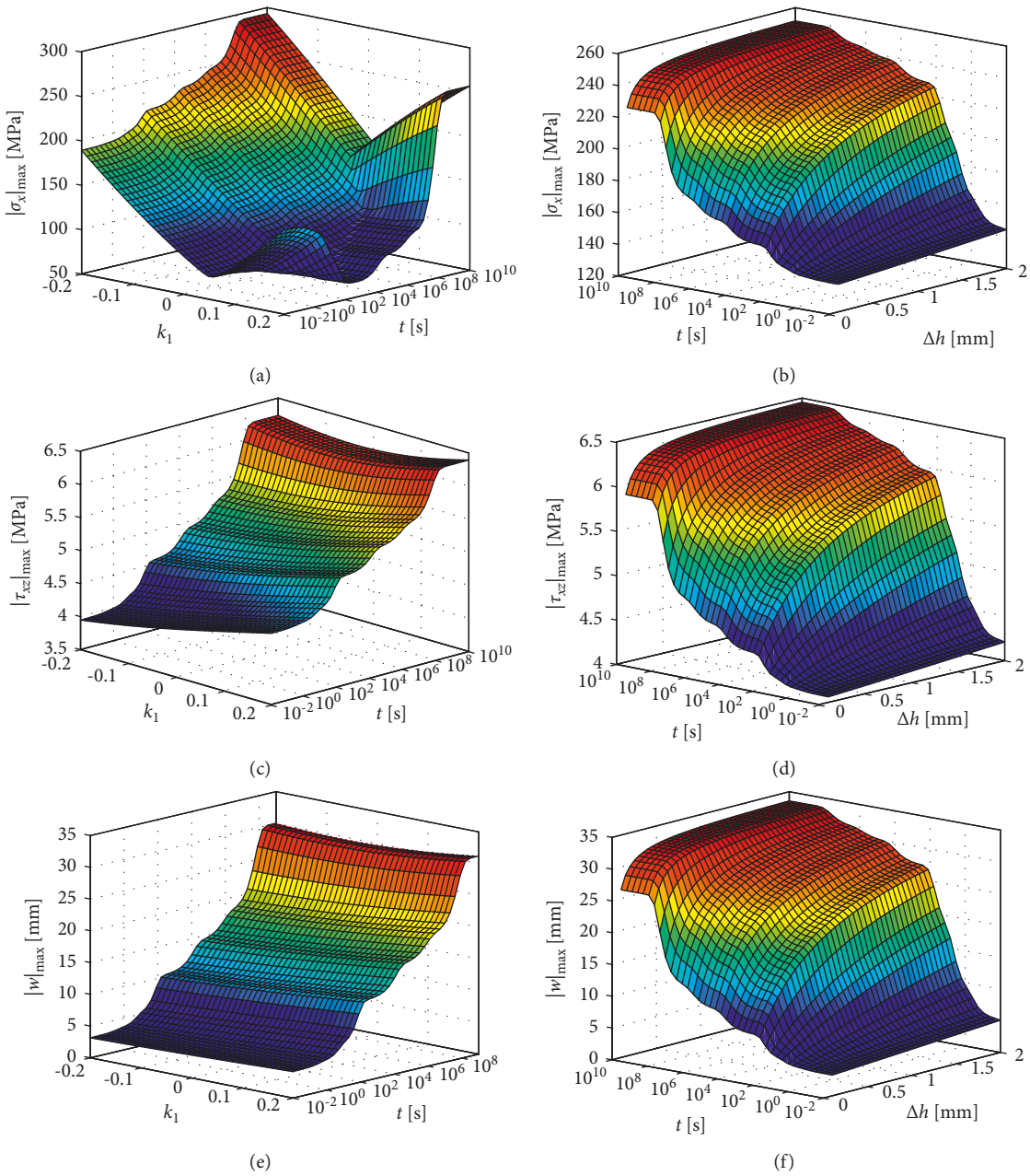

Figure 6: The influence of time and graded index or the interlayer thickness on the maximum value of the normal stress, shear stress, and deflection. (a) $|\sigma_x^i|_{max}$ ($\Delta h = 0.2$ mm), (b) $|\sigma_x^i|_{max}$ ($k_1 = -0.1$), (c) $|\tau_{xz}^i|_{max}$ ($\Delta h = 0.2$ mm), (d) $|\tau_{xz}^i|_{max}$ ($k_1 = -0.1$), (e) $|w^i|_{max}$ ($\Delta h = 0.2$ mm), and (f) $|w^i|_{max}$ ($k_1 = -0.1$).

results shown in Figures 5(b) and 5(c), the decline of k_1 reduces the maximum value of $|\tau_{xz}^i|$ and $|w^i|$ but enlarges that of $|\sigma_x^i|$. As k_1 goes down from 0.2 to -0.2, $|\tau_{xz}^i|_{max}$ and $|w^i|_{max}$ fall by 10.0% and 15.7%, respectively, while $|\sigma_x^i|_{max}$ increases by 156.7%. In the other word, the stress and displacement distribution can be optimized by adjusting the graded index.

Figure 6 shows the influences of t, k_1, and Δh on the maximum value of the stress and displacement. The parameters are fixed at the same as those in Figure 5, except t, k_1 and Δh are variable. It can be seen from Figure 6 that, as $k_1 = -0.1$, $|\sigma_x^i|_{max}$, $|\tau_{xz}^i|_{max}$, and $|w^i|_{max}$ increase monotonously and keeps invariant as t or Δh increases. Due to the increase of t and Δh resulting in a reduced shear modulus of the interlayer, and as $t \longrightarrow \infty$, $G^*(t)$ approaches to the fixed value G_∞^*. Similarly, $|\tau_{xz}^i|_{max}$ and $|w^i|_{max}$ increase monotonously and tend to definite values with the increase of k_1 or t as $\Delta h = 0.2$ mm, which results from that the difference in elastic modulus between the adjacent layer surfaces grows gradually as k_1 increases. For a given t, $|\sigma_x^i|_{max}$ decreases first and then increases as k_1 grows, which is owing to the fact that the location of $|\sigma_x^i|_{max}$ transfers from the outer surface of the facial layer to the inner surface in the early stage, while in the medium or long term, the location of

$|\sigma_x^i|_{\max}$ transfers from the facial layer to the core layer as k_1 increases. Similarly, for a small certain k_1, $|\sigma_x^i|_{\max}$ increases monotonously with t, while for a large k_1, $|\sigma_x^i|_{\max}$ firstly decreases and then increases as t goes on, which is due to the transfer of the $|\sigma_x^i|_{\max}$ location from the facial layer to the core layer.

4. Conclusion

The elasticity theory with the recursive matrix method was proposed to analyze the time-dependent behavior of the layered functionally graded plates with viscoelastic interlayer. The following conclusions can be provided:

(1) In the thin plate case, the KL solution with small graded index approaches the present one. Since the transverse shear deformation is neglected and the neutral plane gradually deviates from the middle plane, the relative errors increase gradually as length-to-height ratio or graded index increases.

(2) As time goes on, the influence of the interlayer shear modulus degeneration for the adhesive bonding case is obvious, which leads to the reduced interface shear stress and the increased interfacial slip as well as the greater deflection.

(3) By adjusting the graded index, the stress and displacement distribution of the case with fixed material consumption can be optimized and the location of the maximum value of the normal stress transfers between the facial layer and the core layer. The maximum value of deflection and shear stress decreases with the reduction of the graded index and the interlayer thickness.

Appendix

A. Details of Coefficients in General Solutions

In (13) and (14), the details of g_{mn}^{ij} ($j = 1$–6) and f_{mn}^{il} ($l = 1$–4) are given as follows:

$$
\begin{aligned}
g_{mn}^{i1} &= \frac{1}{2}\frac{\sqrt{(1-\mu_i)\left[r_{mn,2}^i(1-\mu_i)+4r_{mn,3}^i\right]}-k_i(1-\mu_i)}{1-\mu_i},\\
g_{mn}^{i2} &= -\frac{1}{2}\frac{\sqrt{(1-\mu_i)\left[r_{mn,2}^i(1-\mu_i)+4r_{mn,3}^i\right]}+k_i(1-\mu_i)}{1-\mu_i},\\
g_{mn}^{i3} &= \frac{1}{2}\frac{\sqrt{(1-\mu_i)\left[r_{mn,2}^i(1-\mu_i)-4r_{mn,3}^i\right]}-k_i(1-\mu_i)}{1-\mu_i},\\
g_{mn}^{i4} &= \frac{1}{2}\frac{\sqrt{(1-\mu_i)\left[r_{mn,2}^i(1-\mu_i)-4r_{mn,3}^i\right]}-k_i(1-\mu_i)}{1-\mu_i},\\
g_{mn}^{i5} &= \frac{1}{2}\left(\sqrt{r_{mn,2}^i}-k_i\right),\\
g_{mn}^{i6} &= -\frac{1}{2}\left(\sqrt{r_{mn,2}^i}+k_i\right),\\
f_{mn}^{i1} &= \frac{T_{mn}^i}{\left\{-8(\mu_i-1)^4 r_{mn,1}^i r_{mn,2}^i\sqrt{\left[4r_{mn,3}^i+r_{mn,2}^i(1-\mu_i)\right](1-\mu_i)}+\left[4r_{mn,3}^i(1-\mu_i)+(1-\mu_i)^2 r_{mn,2}^i\right]^{3/2}\left[8k_i^2\mu_i^3+\left(-4\phi_{mn}^2-17k_i^2\right)\mu_i^2-r_{mn,2}^i+4r_{mn,3}^i+\left(8\phi_{mn}^2+10k_i^2-4r_{mn,3}^i\right)\mu_i\right]-64(\mu_i-1)^4(\mu_i-1/4)k_i^3\mu_i\left(\phi_{mn}^2-2r_{mn,3}^i\right)\right\}},\\
f_{mn}^{i2} &= \frac{T_{mn}^i}{\left\{8(\mu_i-1)^4 r_{mn,1}^i r_{mn,2}^i\sqrt{\left[4r_{mn,3}^i+r_{mn,2}^i(1-\mu_i)\right](1-\mu_i)}-\left[4r_{mn,3}^i(1-\mu_i)+(1-\mu_i)^2 r_{mn,2}^i\right]^{3/2}\left[8k_i^2\mu_i^3+\left(-4\phi_{mn}^2-17k_i^2\right)\mu_i^2-r_{mn,2}^i+4r_{mn,3}^i+\left(8\phi_{mn}^2+10k_i^2-4r_{mn,3}^i\right)\mu_i\right]-64(\mu_i-1)^4(\mu_i-1/4)k_i^3\mu_i\left(\phi_{mn}^2-2r_{mn,3}^i\right)\right\}},\\
f_{mn}^{i3} &= \frac{T_{mn}^i}{\left\{-8(\mu_i-1)^4 r_{mn,1}^i r_{mn,2}^i\sqrt{\left[-4r_{mn,3}^i+r_{mn,2}^i(1-\mu_i)\right](1-\mu_i)}+\left[4r_{mn,3}^i(\mu_i-1)+(1-\mu_i)^2 r_{mn,2}^i\right]^{3/2}\left[8k_i^2\mu_i^3+\left(-4\phi_{mn}^2-17k_i^2\right)\mu_i^2-r_{mn,2}^i-4r_{mn,3}^i+\left(8\phi_{mn}^2+10k_i^2+4r_{mn,3}^i\right)\mu_i\right]-64(\mu_i-1)^4(\mu_i-1/4)k_i^3\mu_i\left(\phi_{mn}^2+2r_{mn,3}^i\right)\right\}},\\
f_{mn}^{i4} &= \frac{T_{mn}^i}{\left\{8(\mu_i-1)^4 r_{mn,1}^i r_{mn,2}^i\sqrt{\left[-4r_{mn,3}^i+r_{mn,2}^i(1-\mu_i)\right](1-\mu_i)}-\left[4r_{mn,3}^i(\mu_i-1)+(1-\mu_i)^2 r_{mn,2}^i\right]^{3/2}\left[8k_i^2\mu_i^3+\left(-4\phi_{mn}^2-17k_i^2\right)\mu_i^2-r_{mn,2}^i-4r_{mn,3}^i+\left(8\phi_{mn}^2+10k_i^2+4r_{mn,3}^i\right)\mu_i\right]-64(\mu_i-1)^4(\mu_i-1/4)k_i^3\mu_i\left(\phi_{mn}^2+2r_{mn,3}^i\right)\right\}},\\
&\quad i = 1,2,\ldots,p,\ m,\ n = 1,2,3\ldots,
\end{aligned}
\tag{A.1}
$$

where

$$
\begin{aligned}
\phi_{mn} &= \sqrt{\alpha_m^2+\beta_n^2},\\
r_{mn,1}^i &= k_i^2\mu_i-\frac{1}{8}k_i^2-\frac{1}{2}\beta_n^2-\frac{1}{2}\alpha_m^2,\\
r_{mn,2}^i &= k_i^2+4\alpha_m^2+4\beta_n^2,\\
r_{mn,3}^i &= \sqrt{k_i^2\mu_i\left(\alpha_m^2+\beta_n^2\right)(\mu_i-1)},\\
T_{mn}^i &= 128\mu_i(\mu_i-1)^4 k_i^2\alpha_m\left(k_i^2\mu_i^2-k_i^2\mu_i-\frac{1}{4}\phi_{mn}^2\right).
\end{aligned}
\tag{A.2}
$$

B. Details of Elements in Coefficient Matrix

$\mathbf{M}_m^i(z)$ in (22) is with the following nonzero elements:

$$
\begin{aligned}
&R_{mn}^{11}(z)=e^{g_{mn,1}^i z},\ R_{mn}^{12}(z)=e^{g_{mn,2}^i z},\ R_{mn}^{13}(z)=e^{g_{mn,3}^i z},\ R_{mn}^{14}(z)=e^{g_{mn,4}^i z},\ R_{mn}^{15}(z)=e^{g_{mn,5}^i z},\ R_{mn}^{16}(z)=e^{g_{mn,6}^i z},\\
&R_{mn}^{21}(z)=\frac{\beta_n}{\alpha_m}e^{g_{mn,1}^i z},\ R_{mn}^{22}(z)=\frac{\beta_n}{\alpha_m}e^{g_{mn,2}^i z},\ R_{mn}^{23}(z)=\frac{\beta_n}{\alpha_m}e^{g_{mn,3}^i z},\ R_{mn}^{24}(z)=\frac{\beta_n}{\alpha_m}e^{g_{mn,4}^i z},\ R_{mn}^{25}(z)=-\frac{\alpha_m}{\beta_n}e^{g_{mn,5}^i z},\ R_{mn}^{26}(z)=-\frac{\alpha_m}{\beta_n}e^{g_{mn,6}^i z},\\
&R_{mn}^{31}(z)=\frac{f_{mn,1}^i}{T_{mn}^i}e^{g_{mn,1}^i z},\ R_{mn}^{32}(z)=\frac{f_{mn,1}^i}{T_{mn}^i}e^{g_{mn,2}^i z},\ R_{mn}^{33}(z)=\frac{f_{mn,1}^i}{T_{mn}^i}e^{g_{mn,3}^i z},\ R_{mn}^{34}(z)=\frac{f_{mn,1}^i}{T_{mn}^i}e^{g_{mn,4}^i z},\\
&R_{mn}^{41}(z)=\frac{E_0^i e^{k_i(z-d_0^i)}}{(1+\mu_i)(1-2\mu_i)}\left[-\alpha_m\mu_i-\frac{\mu_i\beta_n^2}{\alpha_m}+\frac{(1-\mu_i)g_{mn,1}^i f_{mn,1}^i}{T_{mn}^i}\right]e^{g_{mn,1}^i z},\\
&R_{mn}^{42}(z)=\frac{E_0^i e^{k_i(z-d_0^i)}}{(1+\mu_i)(1-2\mu_i)}\left[-\alpha_m\mu_i-\frac{\mu_i\beta_n^2}{\alpha_m}+\frac{(1-\mu_i)g_{mn,2}^i f_{mn,2}^i}{T_{mn}^i}\right]e^{g_{mn,2}^i z},\\
&R_{mn}^{43}(z)=\frac{E_0^i e^{k_i(z-d_0^i)}}{(1+\mu_i)(1-2\mu_i)}\left[-\alpha_m\mu_i-\frac{\mu_i\beta_n^2}{\alpha_m}+\frac{(1-\mu_i)g_{mn,3}^i f_{mn,3}^i}{T_{mn}^i}\right]e^{g_{mn,3}^i z},\\
&R_{mn}^{44}(z)=\frac{E_0^i e^{k_i(z-d_0^i)}}{(1+\mu_i)(1-2\mu_i)}\left[-\alpha_m\mu_i-\frac{\mu_i\beta_n^2}{\alpha_m}+\frac{(1-\mu_i)g_{mn,4}^i f_{mn,4}^i}{T_{mn}^i}\right]e^{g_{mn,4}^i z},\\
&R_{mn}^{51}(z)=\frac{E_0^i e^{k_i(z-d_0^i)}}{2(1+\mu_i)}\left(g_{mn,1}^i+\frac{\alpha_m f_{mn,1}^i}{T_{mn}^i}\right)e^{g_{mn,1}^i z},\\
&R_{mn}^{52}(z)=\frac{E_0^i e^{k_i(z-d_0^i)}}{2(1+\mu_i)}\left(g_{mn,2}^i+\frac{\alpha_m f_{mn,2}^i}{T_{mn}^i}\right)e^{g_{mn,2}^i z},\\
&R_{mn}^{53}(z)=\frac{E_0^i e^{k_i(z-d_0^i)}}{2(1+\mu_i)}\left(g_{mn,3}^i+\frac{\alpha_m f_{mn,3}^i}{T_{mn}^i}\right)e^{g_{mn,3}^i z},\\
&R_{mn}^{54}(z)=\frac{E_0^i e^{k_i(z-d_0^i)}}{2(1+\mu_i)}\left(g_{mn,4}^i+\frac{\alpha_m f_{mn,4}^i}{T_{mn}^i}\right)e^{g_{mn,4}^i z},\\
&R_{mn}^{55}(z)=\frac{E_0^i e^{k_i(z-d_0^i)}}{2(1+\mu_i)}g_{mn,5}^i e^{g_{mn,5}^i z},\\
&R_{mn}^{56}(z)=\frac{E_0^i e^{k_i(z-d_0^i)}}{2(1+\mu_i)}g_{mn,6}^i e^{g_{mn,6}^i z},\\
&R_{mn}^{61}(z)=\frac{E_0^i e^{k_i(z-d_0^i)}}{2(1+\mu_i)}\left[\frac{\beta_n g_{mn,1}^i}{\alpha_m}+\frac{\beta_n f_{mn,1}^i}{T_{mn}^i}\right]e^{g_{mn,1}^i z},\\
&R_{mn}^{62}(z)=\frac{E_0^i e^{k_i(z-d_0^i)}}{2(1+\mu_i)}\left[\frac{\beta_n g_{mn,2}^i}{\alpha_m}+\frac{\beta_n f_{mn,2}^i}{T_{mn}^i}\right]e^{g_{mn,2}^i z},\\
&R_{mn}^{63}(z)=\frac{E_0^i e^{k_i(z-d_0^i)}}{2(1+\mu_i)}\left[\frac{\beta_n g_{mn,3}^i}{\alpha_m}+\frac{\beta_n f_{mn,3}^i}{T_{mn}^i}\right]e^{g_{mn,3}^i z},\\
&R_{mn}^{64}(z)=\frac{E_0^i e^{k_i(z-d_0^i)}}{2(1+\mu_i)}\left[\frac{\beta_n g_{mn,4}^i}{\alpha_m}+\frac{\beta_n f_{mn,4}^i}{T_{mn}^i}\right]e^{g_{mn,4}^i z},\\
&R_{mn}^{65}(z)=-\frac{E_0^i e^{k_i(z-d_0^i)}}{2(1+\mu_i)}\left(\frac{\alpha_m g_{mn,5}^i}{\beta_n}\right)e^{g_{mn,5}^i z},\\
&R_{mn}^{66}(z)=\frac{E_0^i e^{k_i(z-d_0^i)}}{2(1+\mu_i)}\left(\frac{\alpha_m g_{mn,6}^i}{\beta_n}\right)e^{g_{mn,6}^i z}.
\end{aligned}
\tag{B.1}
$$

Data Availability

The raw/processed data required to reproduce these findings cannot be shared at this time as the data also form part of an ongoing study.

Conflicts of Interest

The authors declare no conflicts of interest with respect to the research, authorship, and/or publication of this article.

Acknowledgments

This research was financially supported by National Natural Science Foundation of China (no. 52108220) and Natural Science Foundation of Jiangsu Province (no. BK20190668).

References

[1] F. Moleiro, E. Carrera, A. J. M. Ferreira, and J. N. Reddy, "Hygro-thermo-mechanical modelling and analysis of multilayered plates with embedded functionally graded material layers," *Composite Structures*, vol. 233, Article ID 111442, 2020.

[2] V. Gulizzi, I. Benedetti, and A. Milazzo, "A high-resolution layer-wise discontinuous Galerkin formulation for multilayered composite plates," *Composite Structures*, vol. 242, Article ID 112137, 2020.

[3] L. V. Tran and S. E. Kim, "Static and free vibration analyses of multilayered plates by a higher-order shear and normal deformation theory and isogeometric analysis," *Thin-Walled Structures*, vol. 130, pp. 622–640, 2018.

[4] I. Benedetti and A. Milazzo, "Advanced models for smart multilayered plates based on Reissner Mixed Variational Theorem," *Composites Part B: Engineering*, vol. 119, pp. 215–229, 2017.

[5] L. Galuppi and G. Royer-Carfagni, "Laminated beams with viscoelastic interlayer," *International Journal of Solids and Structures*, vol. 49, no. 18, pp. 2637–2645, 2012.

[6] P. Foraboschi, "Analytical model for laminated-glass plate," *Composites Part B: Engineering*, vol. 43, no. 5, pp. 2094–2106, 2012.

[7] A. Tounsi, M. S. A. Houari, S. Benyoucef, and E. A. A. Bedia, "A refined trigonometric shear deformation theory for thermoelastic bending of functionally graded sandwich plates," *Aerospace Science and Technology*, vol. 24, no. 1, pp. 209–220, 2013.

[8] R. Xu and Y. F. Wu, "Two-dimensional analytical solutions of simply supported composite beams with interlayer slips," *International Journal of Solids and Structures*, vol. 44, no. 1, pp. 165–175, 2007.

[9] A. Zemanová, J. Zeman, and M. Šejnoha, "Comparison of viscoelastic finite element models for laminated glass beams," *International Journal of Mechanical Sciences*, vol. 131-132, pp. 380–395, 2017.

[10] M. K. Apalak and R. Gunes, "Thermal residual stresses in an adhesively-bonded functionally graded single-lap joint," *Journal of Adhesion Science and Technology*, vol. 20, no. 12, pp. 1295–1320, 2006.

[11] R. M. J. Groh and P. M. Weaver, "On displacement-based and mixed-variational equivalent single layer theories for modelling highly heterogeneous laminated beams," *International Journal of Solids and Structures*, vol. 59, pp. 147–170, 2015.

[12] K. Susanto, "Vibration analysis of piezoelectric laminated slightly curved beams using distributed transfer function method," *International Journal of Solids and Structures*, vol. 46, no. 6, pp. 1564–1573, 2009.

[13] N. T. Khiem, H. T. Tran, and D. Nam, "Modal analysis of cracked continuous Timoshenko beam made of functionally graded material," *Mechanics Based Design of Structures and Machines*, vol. 48, no. 4, pp. 459–479, 2020.

[14] A. M. Zenkour and R. A. Alghanmi, "Bending of exponentially graded plates integrated with piezoelectric fiber-reinforced composite actuators resting on elastic foundations," *European Journal of Mechanics - A: Solids*, vol. 75, pp. 461–471, 2019.

[15] S. K. Jalali, M. H. Naei, and A. Poorsolhjouy, "Thermal stability analysis of circular functionally graded sandwich plates of variable thickness using pseudo-spectral method," *Materials & Design*, vol. 31, no. 10, pp. 4755–4763, 2010.

[16] Y. Zhang, G. Jin, M. Chen, T. Ye, C. Yang, and Y. Yin, "Free vibration and damping analysis of porous functionally graded sandwich plates with a viscoelastic core," *Composite Structures*, vol. 244, Article ID 112298, 2020.

[17] M. H. G. Babaki and M. Shakouri, "Free and Forced Vibration of sandwich Plates with Electrorheological Core and Functionally Graded Face Layers," *Mechanics Based Design Structures and Machines*, vol. 49, no. 5, pp. 689–706, 2019.

[18] M. Dorduncu, "Stress analysis of sandwich plates with functionally graded cores using peridynamic differential operator and refined zigzag theory," *Thin-Walled Structures*, vol. 146, Article ID 106468, 2020.

[19] R. Gunes, M. A. Kemal, and I. Ozkes, "Free vibration analysis of adhesively bonded single lap joints with wide and narrow functionally graded plates," *Composite Structures*, vol. 92, no. 1, pp. 1–17, 2010.

[20] M. D. Demirbas and M. K. Apalak, "Investigation of the thermo-elastic response of adhesively bonded two-dimensional functionally graded circular plates based on theory of elasticity," *Iranian Journal of Science and Technology, Transactions of Mechanical Engineering*, vol. 42, no. 4, pp. 415–433, 2018.

[21] F. Tornabene, M. Viscoti, and M. Dinitri, "Equivalent single layer higher order theory based on a weak formulation for the dynamic analysis of anisotropic doubly-curved shells with arbitrary geometry and variable thickness," *Thin-Walled Structures*, vol. 174, Article ID 109119, 2022.

[22] D. D. Li, Z. B. Deng, G. P. Chen, H. Xiao, and L. Zhu, "Thermomechanical bending analysis of sandwich plates with both functionally graded face sheets and functionally graded core," *Composite Structures*, vol. 169, pp. 29–41, 2017.

[23] X. Wang, Z. Wang, T. Zeng, S. Cheng, and F. Yang, "Exact analytical solution for steady-state heat transfer in functionally graded sandwich slabs with convective-radiative boundary conditions," *Composite Structures*, vol. 192, pp. 379–386, 2018.

[24] F. Tornabene, M. Viscoti, M. Dinitri, and J. N. Reddy, "Higher order theories for the vibration study of doubly-curved anisotropic shells with a variable thickness and isogeometric mapped geometry," *Composite Structures*, vol. 267, Article ID 113829, 2021.

[25] F. Tornabene, M. Viscoti, and R. Dimitri, "Generalized higher order layerwise theory for the dynamic study of anisotropic doubly -curved shells with a mapped geometry," *Engineering Analysis with Boundary Elements*, vol. 134, pp. 147–183, 2022.

[26] S. Ghimire and J. Chen, "An extended cohesive damage model study of geometrical ratio effects on failure mechanisms of

functionally graded sandwiches with multi-layered cores," *Composite Structures*, vol. 224, Article ID 110999, 2019.

[27] L. C. Trinh, T. P. Vo, H. T. Thai, T. K. Nguyen, and P. Keerthan, "State-space Levy solution for size-dependent static, free vibration and buckling behaviours of functionally graded sandwich plates," *Composites Part B: Engineering*, vol. 149, pp. 144–164, 2018.

[28] K. Khorshidi and M. Karimi, "Flutter analysis of sandwich plates with functionally graded face sheets in thermal environment," *Aerospace Science and Technology*, vol. 95, Article ID 105461, 2019.

[29] S. Nikbakht, S. J. Salami, and M. Shakeri, "A 3D full layer-wise method for yield achievement in Functionally Graded Sandwich Plates with general boundary conditions," *European Journal of Mechanics - A: Solids*, vol. 75, pp. 330–347, 2019.

[30] F. Tornabene, "Free vibration analysis of functionally graded conical, cylindrical shell and annular plate structures with a four-parameter power-law distribution," *Computer Methods in Applied Mechanics and Engineering*, vol. 198, pp. 37–40, 2009.